Journal of Power Sources 195 (2010) 8251–8257

Contents lists available at ScienceDirect

Journal of Power Sources

journal homepage: www.elsevier.com/locate/jpowsour

XPS and ToF-SIMS study of Sn–Co alloy thin films as anode for lithium ion battery

Jun-Tao Li[a], Jolanta Swiatowska[b], Antoine Seyeux[b], Ling Huang[c], Vincent Maurice[b,*], Shi-Gang Sun[c,*], Philippe Marcus[b,*]

[a] School of Energy Research, Xiamen University, Xiamen 361005, China
[b] Laboratoire de Physico-Chimie des Surfaces, CNRS (UMR 7045), Ecole Nationale Supérieure de Chimie de Paris (Chimie-ParisTech), 11 rue Pierre et Marie Curie, 75231 Paris Cedex 05, France
[c] State Key Laboratory of Physical Chemistry of Solid Surfaces, Department of Chemistry, College of Chemistry and Chemical Engineering, Xiamen University, Xiamen 361005, China

ARTICLE INFO

Article history:
Received 28 December 2009
Received in revised form 7 July 2010
Accepted 18 July 2010
Available online 23 July 2010

Keywords:
XPS
ToF-SIMS
Sn–Co alloy
Anode material
Lithium ion battery
SEI layer

ABSTRACT

Sn–Co alloy films were prepared by electroplating on copper and used as anode material of lithium ion battery. Cyclic voltammetry and galvanostatic discharge/charge measurements were combined with surface analysis by X-ray photoelectron spectroscopy (XPS) and time-of-flight secondary ion mass spectrometry (ToF-SIMS). The results show the buildup of a solid electrolyte interphase (SEI) layer formed by reductive decomposition of electrolyte during the first Li–Sn alloying cycle. The layer is constituted of a mixture of Li_2CO_3, $ROCO_2Li$, lithium oxalates, and/or ROLi, and its chemical composition is modified during the electrochemical multi-cycling process with increase of the Li_2CO_3 content. Multi-cycling also fractures the SEI layer. ToF-SIMS results revealed an incomplete initial alloying process of lithium ion with Sn, limited by mass transport through a Co layer and dividing the Sn–Co layer alloy into a fully lithiated outer part and an essentially non-lithiated inner layer during the first discharge. The volume expansion/shrink associated with the alloying/dealloying reaction irreversibly cracks and splits up the Sn–Co alloy into particles with interstitials voids filled by the SEI layer. Multi-cycling amplifies this division of the Sn–Co layer without material loss and stabilizes discharge/charge capacity.

1. Introduction

Sn-based alloys are considered to be very promising alternative anodes for lithium ion batteries (LIBs) because of their higher specific capacity than commercially used carbon anodes and their better cycling ability than pure tin anodes [1–3]. Moreover, Sn-based alloy anodes do not suffer from the so-called co-intercalation observed on graphite anodes [4]. The Sn-based anodes alloy two or more elements. The active component, tin, reacts with lithium, whereas the other elements act as an electrochemically inactive buffer accommodating the volume changes. However, large volume changes are inevitably associated with alloying/dealloying reactions, and are the main origin for severe stress-induced fracture, which leads to the loss of contact between particles and significant capacity fading on cycling. Nanostructures, core-shell structures and amorphous structures of Sn-based alloy electrodes have been synthesized in order to improve their durability and to minimize dimensional changes and pulverization failure induced by discharging/charging [5–8].

Alloying with cobalt is expected to increase the ductibility of the material and the volume variation accommodation, to stabilize the reduced tin atoms in the lithiation stage, and thus to improve the electrochemical cycling stability [9]. The interest for Sn–Co alloy anodes has risen since the commercialization by a Japanese company of the Co–Sn–C component anode, composed of small grains of Sn–Co in a C matrix [10]. Co–Sn binary [11–16] and Sn–Co based ternary [16–21] alloys synthesized by various methods have been the subject of many electrochemical studies. It has been reported that four intermetallic phases are present in the Co–Sn binary alloy: CoSn, $CoSn_2$, Co_3Sn_2 and $CoSn_3$ [22,23]. The alloying/dealloying reaction is the following:

$$SnCo_y + xe^- + xLi^+ \leftrightarrow Li_xSn + yCo \quad (x < 4.4) \tag{1}$$

Despite the progress of electrochemical performance of Sn–Co binary anodes, the mechanisms of interfacial reactions are not yet completely known. Questions still remain regarding the formation, stability, variation and composition of the solid electrode interphase (SEI) layer, as well as the morphological and phase structural changes of Sn–Co alloy anodes during discharge/charge, which are key issues for the cycling ability, the lifetime, the chemical and physical stability and the reversible capacity of LIBs. In addition, the electrochemical reactions always start at the interface between the

* Corresponding authors. Tel.: +33 01 44 27 67 38; fax: +33 01 46 34 07 53.
E-mail addresses: vincent-maurice@chimie-paristech.fr (V. Maurice), sgsun@xmu.edu.cn (S.-G. Sun), philippe-marcus@chimie-paristech.fr (P. Marcus).

0378-7753/$ – see front matter © 2010 Elsevier B.V. All rights reserved.
doi:10.1016/j.jpowsour.2010.07.043

electrode and the electrolyte. Therefore, a better understanding of the interfacial reactions as well as the phenomena occurring inside the bulk electrode are prerequisite for further improvements of the Sn–Co alloy anodes for their commercial application. Up to now, the morphological and phase structural changes on Sn-based anodes have been extensively studied by in situ XRD and Mossbauer spectroscopy, which could probe the structure of electrode materials at the atomic level [24–27]. The application of the X-ray photoelectron spectroscopy (XPS) to characterize cycled Sn-based alloys has been reported by several research groups [28–32]. In addition, the interfacial reactions on the tin anode have been investigated by in situ Fourier transform infrared reflection spectroscopy (in situ FTIRS) [33–34].

XPS has been applied to investigate the chemical composition of the SEI layer formed on various electrode materials by analysis of the valence band and the core level regions of C, O, Li and F [35–40]. However, this technique provides information on the chemical composition of the first few nanometers at the electrode surface whereas some of the interesting issues relate to its bulk composition. Secondary ion mass spectrometry (SIMS) has an excellent sensitivity to lithium [41]. More recently, Time-of-Flight SIMS (ToF-SIMS) has been applied to depth-profile cycled electrode materials with a good depth resolution bringing information about the SEI layer and the distribution of species in the bulk materials [38,42–45].

Here we present a combined investigation by XPS and ToF-SIMS of electroplated Sn–Co alloy anode cycled in 1 M $LiClO_4$/PC. The interfacial mechanisms related to the formation and modification of the SEI layer during cycling are addressed, as well as the morphological changes of the electroplated layer related to the alloying/dealloying interfacial reaction.

2. Experimental

2.1. Preparation of Sn–Co anode

Electroplating of Sn–Co alloy films were carried out on copper foils (area = 2.6 cm^2, l = 0.1 mm) in a bath containing 75 g L^{-1} $Na_2SnO_3{\cdot}3H_2O$, 2.5 g L^{-1} $CoCl_2{\cdot}6H_2O$ and the additives (150 g L^{-1} $C_4H_4O_6KNa{\cdot}4H_2O$, and 20 g L^{-1} $K_3C_6H_5O_7{\cdot}H_2O$), which act as the complexing agents. All these reagents are analytical reagents, and were purchased from Sinapharm Chemical Reagent Co. Ltd. The bath temperature was kept at 55 °C and its pH was adjusted to 7.5 via addition of HCl. The electrolyte was not deaerated. Titanium foil was used as counter and reference electrodes. A constant current density of 1.0 A dm^{-2} was applied for 5 min leading to the deposition of ~1.9 mg of alloyed films. After electroplating, the prepared electrode was transferred to an anhydrous ethanol bath and rinsed in ultrasonic bath for 1 min. The thickness is estimated to be 820 nm by considering the Co–Sn alloy density (ρ = 8.91 g cm^{-3}) [26]. Scanning electron microscopy (SEM) observation and energy dispersive X-ray spectroscopy (EDS) analysis, presented in Fig. 1, illustrate that a continuous Sn–Co alloy film is produced with Sn and Co atomic ratio of 62 and 28%, respectively (~Sn_2Co).

2.2. Electrochemical properties of Sn–Co anode

Cyclic voltammetry (CV) and galvanostatic discharge/charge studies were carried out in a glove box (Jacomex) under Ar atmosphere (O_2 and H_2O < 5 ppm). A conventional three-electrode glass cell was employed with Sn–Co alloy film as working electrode and Li foil (Aldrich) as reference and counter electrodes. All potentials given in this paper are referred versus the Li^+/Li reference electrode. An Autolab (AUT30) potentiostat/galvanostat was used. The electrolyte was an organic, anhydrous solution of 1 M lithium perchlorate in propylene carbonate (1 M $LiClO_4$/PC, Aldrich). After

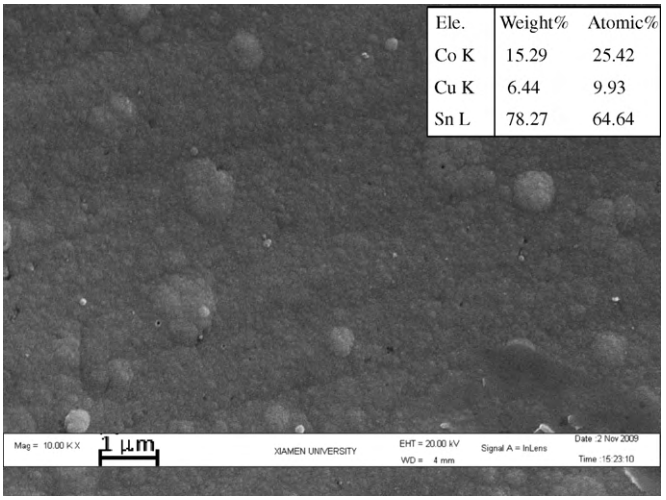

Fig. 1. SEM images and EDX analysis of Sn–Co alloy layer electrode on Cu substrate.

electrochemical treatment, the specimens were emerged from the electrolyte at applied potential, rinsed with anhydrous acetonitrile, dried in Ar flow and transferred directly from the Ar atmosphere of the glove box to the ultra-high vacuum XPS analysis chamber without exposure to air. For ToF-SIMS analysis, the specimen were stored in the glove box and transferred rapidly through laboratory air to the ultra-high vacuum analysis chamber prior to analysis.

2.3. X-ray photoelectron spectroscopy analysis

XPS analysis was carried out with a VG ESCALAB 250 spectrometer equipped with a UHV preparation chamber directly connected to the glove box [40]. Base pressure during analysis was $\sim 1 \times 10^{-9}$ mbar. An Al Kα monochromatized radiation ($h\nu$ = 1486.6 eV) was employed as X-ray source. For all analyses, the take-off angle of the photoelectrons was 90°. High-resolution spectra of the Sn3d, Co2p, O1s, C1s and Li1s core level and valence band (VB) regions were recorded with a pass energy of 20 eV. The data processing (peak fitting) was performed with the Avantage software provided by Thermo Electron Corporation, using a Shirley type background substraction and Gaussian/Lorentzian peak shapes. The binding energies were corrected by setting the C1s hydrocarbon (–CH_2–CH_2– bonds) peak at 285.0 eV.

2.4. Time-of-flight secondary ion mass spectrometry depth profiling

Depth profiles were obtained using a ToF-SIMS 5 spectrometer (IonTof). The spectrometer was run at an operating pressure of $\sim 1 \times 10^{-9}$ mbar. A pulsed 25 keV Bi^+ primary ion source was employed for analysis, delivering 1.8 pA of current over a 100 μm × 100 μm area. Sputtering was done using a 2 keV Cs^+ beam giving a 100 nA target current over a 250 μm × 250 μm area. Data acquisition and post-processing analyses were performed using the Ion-Spec software. Negative ion profiles were recorded and analyzed.

3. Results and discussion

3.1. Electrochemical properties of Sn–Co alloy anode

Fig. 2a depicts some cyclic voltammograms (CVs) of the first 20 cycles recorded on Sn–Co alloy anode at 0.5 mV s^{-1}. The curves are very similar and nearly superimpose except the first cycle. In the first negative-going potential scan (NGPS), the current attributed to

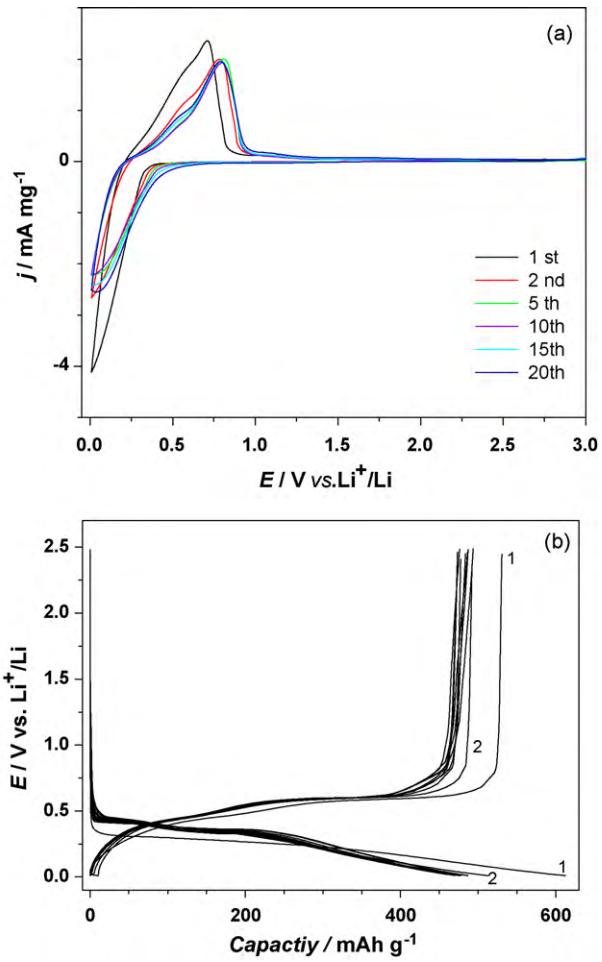

Fig. 2. (a) Selected cyclic voltammograms (CVs) of the first 20 cycles performed in the potential range between 3.0 and 0.02 V, scan rate: 0.50 mV s^{-1}, and (b) the first 10 galvanostatic discharge/charge between 2.5 and 0.01 V, in 1 M $LiClO_4$/PC.

alloying of lithium ion with Sn–Co anode has a threshold at about 0.4 V that is positively shifted in the following NGPSs, indicating an easier initiation of the reaction on the pre-cycled electrode. A cathodic current peak is observed at 0.06 V in the following 19 cycles. In the first positive-going potential scan (PGPS), the anodic current peaks observed at *ca.* 0.55 and 0.7 V are assigned to the dealloying of the Li_xSn phase [9]. The main peak at 0.7 V in the first PGPS is stable at 0.8 V in the following PGPSs, suggesting a more stable Li_xSn phase on the pre-cycled electrode.

The cycling performance of Sn–Co alloy thin film in the first ten cycles at a current rate of 100 mA g^{-1} is illustrated in Fig. 2b. The potential drops rapidly to a plateau of about 0.27 V, and then decreases gradually to 0.02 V in the first discharge process. The plateau and slope correspond to the two-step lithiation process of the Sn–Co thin film anode [26]. In the following cycles, the potential plateau at 0.27 V increases to 0.35 V. In the course of lithium dealloying, the variation of curves are similar but with different capacity. Sn–Co alloy thin film anode delivers a first discharge capacity of 610 mAh g^{-1} and charge capacity of 530 mAh g^{-1}, yielding a columbic efficiency of 87%. The following discharge capacity is stable at about 480 mAh g^{-1}.

3.2. XPS analysis of the pristine and cycled Sn–Co alloy samples

Fig. 3 presents the XP Sn3d, Co2p, C1s and O1s core level and VB region spectra for the pristine and cycled samples. The values of the binding energy (E_B), full width at half maximum (FWHM) and relative intensity of the component peaks used to fit the data are compiled in Table 1.

On the pristine sample (spectra a), the Sn3d and Co2p regions display two 5/2–3/2 and 3/2–1/2 spin orbit doublets, respectively. The A and B components of tin, $Sn3d_{5/2A}$ at 484.9 eV and $Sn3d_{5/2B}$ at 486.5 eV, are assigned to metallic tin (Sn(0)) and oxidized tin (Sn(IV)), respectively [30]. The oxide component dominates with a relative intensity of 71.9%. The A and B components of cobalt, i.e. $Co2p_{3/2A}$ at 778.4 eV and $Co2p_{3/2B}$ at 781.0 eV, are also assigned to metallic Co(0) and oxidized cobalt Co(II), respectively [46]. However, the oxide component is minor with a relative intensity of 30.2%. Thus the surface of Sn–Co alloy film is covered by a thin oxide layer resulting from the exposure of sample to atmosphere. The higher relative intensity of tin oxide indicates the preferential oxidation of this element and the enrichment of tin in the oxide layer. This may influence the electrochemical properties of this alloy and its interfacial reactions with electrolyte during the discharge and charge processes.

The VB region spectrum of the sample displays an intense signal at 23–28 eV assigned to the Sn4d core level. The two sets of A and B components are nearly superimposed due to the lower energy separation of the 5/2–3/2 doublet. The peaks at 59.2 and 60.7 eV are assigned to the 3/2–1/2 doublet of the Co3p core level, respectively. Their higher binding energy shoulder is consistent with the presence of oxidized Co.

On the samples submitted to a half cycle (spectrum b) and one cycle (spectrum c), the Sn3d and Co2p peaks signals are completely attenuated by the growth of a surface layer. The Sn4d photoelectrons are still observed because of their higher kinetic energy (i.e. lower attenuation). The Sn3d peaks reappear although attenuated on the sample treated with twenty cycles (spectrum d) but not the Co2p peaks. The attenuation of Sn and Co peaks during the first electrochemical cycle is consistent with the irreversible buildup of the SEI layer by reduction of electrolyte. XPS is then unable to provide any detailed information about the Li–Sn alloying (dealloying) mechanism during the first cycle. However, the Sn3d peak observed after 20 cycles can be used to analyze the multi-cycled alloy film. Its appearance is indicative of the fracture (and possible loss) of the SEI layer after multiple alloying/dealloying reactions. The binding energy (486.3 eV) of $Sn3d_{5/2B}$ component assigned to Sn(IV) remains unchanged compared to that on the pristine sample, suggesting that a tin oxide layer is still present on the delithiated Sn–Co alloy. However, it is interesting to note that the metallic $Sn3d_{5/2A}$ component is shifted to 483.5 eV (−1.4 eV). This shift can be explained by the negative charge of the tin atoms alloyed with Li [28], thereby indicating that lithium ions are trapped in a Li–Sn alloy at the surface of the delithiated multi-cycled electrode.

The C1s core level peaks on pristine and cycled samples are reported in Fig. 3 and Table 1. On the pristine sample, the C1s signal mostly originates from a contamination layer always detected at the extreme surface. The decomposition of C1s peak shows three components, $C1s_A$ (285.0 eV), $C1s_B$ (286.5 eV) and $C1s_C$ (288.8 eV) assigned to $-CH_2-CH_2-$ bonds, C atoms bounded to one O atom (C–O bonds), and C atoms bounded to two O atoms (O=C–O bonds), respectively.

A modified C1s core level is observed on the cycled Sn–Co alloy samples that show four components at 285.0, 286.6/286.7, 288.6–288.8 and 288.8–290.1 eV. The $C1s_A$ peak at 285.0 eV (C–H bonds) does not show any significant change. A new $C1s_D$ peak at 288.8–290.1 eV can be assigned to C atoms bound to three O atoms in carbonate species, which corresponds to Li_2CO_3 and/or lithium alkyl carbonate $ROCO_2Li$ [29]. Such species have been described as the main reductive products of electrolyte and components of the SEI layer [47,48]. The Li_2CO_3 and $ROCO_2Li$ species are distinguishable by their C–O bonding as the former contains a carbon atom that bounds to three oxygen atoms, while the later has an

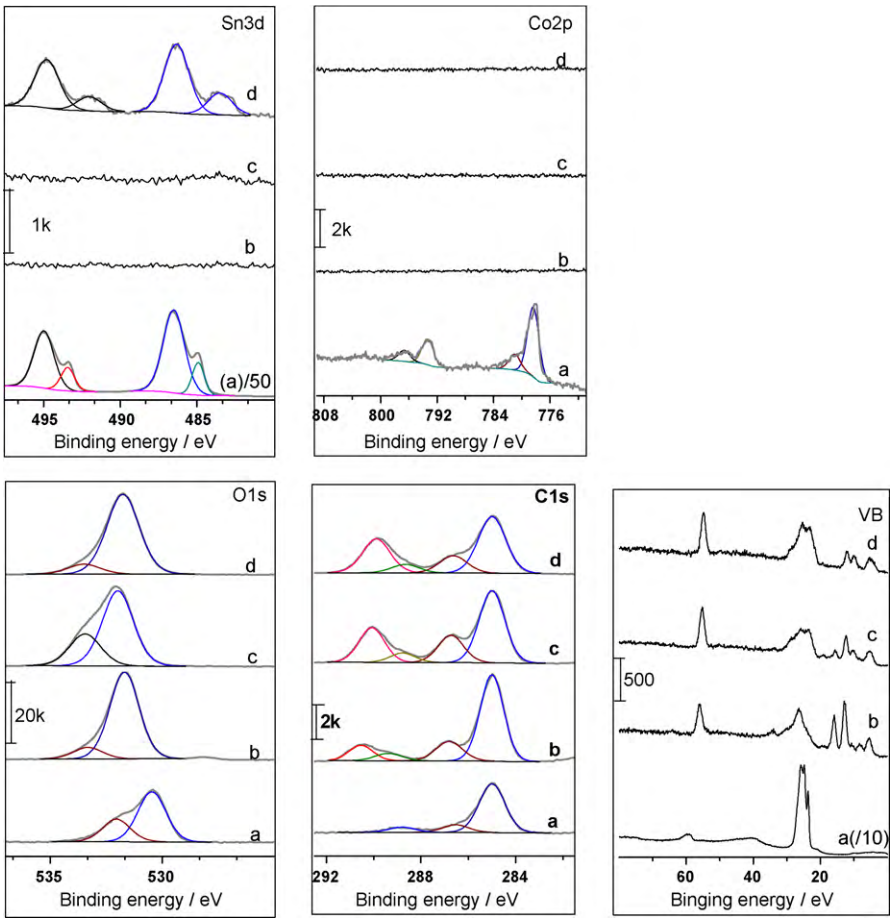

Fig. 3. XP spectra of Sn3d, Co2p, O1s and C1s core level and valence band regions for (a) the pristine Sn–Co alloy, (b) a lithiated Sn–Co alloy anode (potential stopped at 0.02 V in the first CV), (c) a delithiated Sn–Co alloy anode (potential stopped at 3.0 V in the first CV) and (d) a multi-cycled delithiated Sn–Co alloy anode (potential stopped at 3.0 V after 20 CVs).

additional R(C)–O bond besides the carbon bound to three oxygen atoms. The $C1s_B$ at 286.6/286.7 eV, assigned to C atoms bonded to one O atom, corresponds then to lithium alkyl carbonates species ($ROCO_2Li$) and/or lithium alcoholates (ROLi) [28–31]. Its relative intensity is 9.9, 19.1 and 15.0% for samples submitted to half, 1 and 20 cycles, respectively. The relative intensity of the $C1s_D$ peak is accordingly 18.5, 24.1 and 29.1% after half, 1 and 20 cycles. This difference of relative intensities between the $C1s_D$ and $C1s_B$ peaks is caused by the variation of Li_2CO_3 component in the SEI layer. Obviously, the SEI layer is composed partially of Li_2CO_3, and its ratio increases with increasing cycling. Finally, the $C1s_C$ component at 286.6–288.8 eV assigned C atoms bound to two O atoms can be explained by the presence of lithium oxalates [31]. Its relative intensity does not markedly change with cycling.

The O1s core level peak on the pristine sample shows a major $O1s_A$ component at 530.5 eV assigned to oxide anions of the oxide

Table 1
Binding energy (E_B), full-width at half-maximum (FWHM) and relative intensity ratio of the Sn3d, Co2p, C1s, O1s and Li1s peaks for the pristine and the cycled treated Sn–Co alloy samples.

	Pristine			Sample after half cycle			Sample after 1 cycle			Sample after 20 cycles		
	B.E. (eV)	Ratio %	FWHM (eV)	B.E. (eV)	Ratio %	FWHM (eV)	B.E. (eV)	Ratio %	FWHM (eV)	B.E. (eV)	Ratio %	FWHM (eV)
$C1s_A$	285.0	78.7	1.3	285.0	61.7	1.3	285.0	50.3	1.3	285.0	48.5	1.4
$C1s_B$	286.5	12.6	1.3	286.6	9.9	1.3	286.7	19.1	1.3	286.6	15.0	1.4
$C1s_C$	288.8	8.7	1.3	288.6	9.9	1.3	288.8	6.5	1.3	288.7	7.3	1.4
$C1s_D$	–	–	–	289.8	18.5	1.3	290.1	24.1	1.3	289.9	29.1	1.4
$O1s_A$	530.5	69.0	1.5	–	–	–	–	–	–	–	–	–
$O1s_B$	532.1	31.0	1.5	531.7	88.5	1.6	532.0	69.4	1.7	531.8	89.3	1.8
$O1s_D$	–	–	–	533.3	11.5	1.6	533.4	30.6	1.7	533.5	10.7	1.8
$Sn3d_{3/2A}$	493.4	28.9	1.1	–	–	–	–	–	–	490.2	22.8	2.0
$Sn3d_{3/2B}$	495.0	71.1	1.6	–	–	–	–	–	–	494.8	77.2	2.0
$Sn3d_{5/2A}$	484.9	28.1	0.9	–	–	–	–	–	–	483.5	24.2	1.9
$Sn3d_{5/2B}$	486.5	71.9	1.7	–	–	–	–	–	–	486.3	75.8	1.9
$Co2p_{1/2A}$	793.3	69.8	2.0	–	–	–	–	–	–	–	–	–
$Co2p_{1/2B}$	796.6	30.2	2.0	–	–	–	–	–	–	–	–	–
$Co2p_{3/2A}$	778.4	81.3	2.0	–	–	–	–	–	–	–	–	–
$Co2p_{3/2B}$	781.0	18.7	2.0		–	–	–	–	–	–	–	
Li1s	–	–	–	55.8	–	–	55.3	–	–	55.0	–	–

film with an $O1s_B$ shoulder at 532.1 eV attributed to adsorbed hydroxyl groups and water molecules [49,50]. These species most likely originate from the alloy synthesis in aqueous solutions and the sample exposure to ambient conditions. The O1s of the cycled samples consists of different peaks. The $O1s_A$ component at 530.5 eV is fully attenuated by the growth of the SEI layer, in agreement with the attenuation of the Sn and Co peaks. The $O1s_B$ component at 531.7–532.0 eV becomes the major component and is assigned to carbonate species [37]. A new $O1s_C$ component appears at 533.3/533.5 eV on the cycled samples and can be assigned to the presence of Li–alkyl carbonates ($ROCO_2Li$) and/or Li–alkoxides ($R–CH_2OLi$). A new peak is also observed at 55.0–55.8 eV in the VB region on the cycled samples, which is ascribed to Li1s originating from Li_2CO_3, $ROCO_2Li$ and/or Li salts.

It can be concluded form these XPS data that the SEI layer formed by reductive decomposition of the electrolyte leads to complete attenuation of the Sn3d and Co2p core levels already after the first half cycle. The SEI layer is composed of a mixture of Li_2CO_3, $ROCO_2Li$, lithium oxalates, and/or lithium alcoholates (ROLi) and its chemical composition is modified during the electrochemical multi-cycling process with increase of the Li_2CO_3 content. The reduction of the PC molecule to Li_2CO_3 is possibly promoted by multi-cycling since it requires two electrons whereas reduction to $ROCO_2Li$ requires only one electron. Multi-cycling also fractures the SEI layer as indicated by the re-appearance of the Sn3d core level after 20 cycles. Trapping of Li ions alloyed to Sn is then observed in the delithiated state with no Co present at the surface, showing the enrichment of Sn at the surface of the multi-cycled alloy. Li ion trapping in cycled Sn-based anodes was previously observed by XPS and identified as a cause of irreversible charge capacity [28,30].

3.3. ToF-SIMS depth profile analysis of pristine and (de)lithiated Sn–Co samples

Figs. 4–7 shows the depth profiles of the Sn-containing ions ($^{237.8}Sn_2^-$, $^{117.9}Sn^-$, $^{119.9}Sn^-$), Co-containing ions ($^{58.9}Co^-$, $^{117.9}Co_2^-$), Cu-containing ions ($^{62.9}Cu^-$, $^{125.9}Cu_2^-$), $^{7.0}Li^-$, $^{12}C^-$ and $^{18}O^-$ ions recorded on the pristine and cycled samples. The intensity is reported using a logarithmic scale in order to magnify the low-intensity signals. The variation of the ion intensity with sputter time reflects the variation of the in-depth concentration but it is also dependent on the matrix from which the ions are emitted.

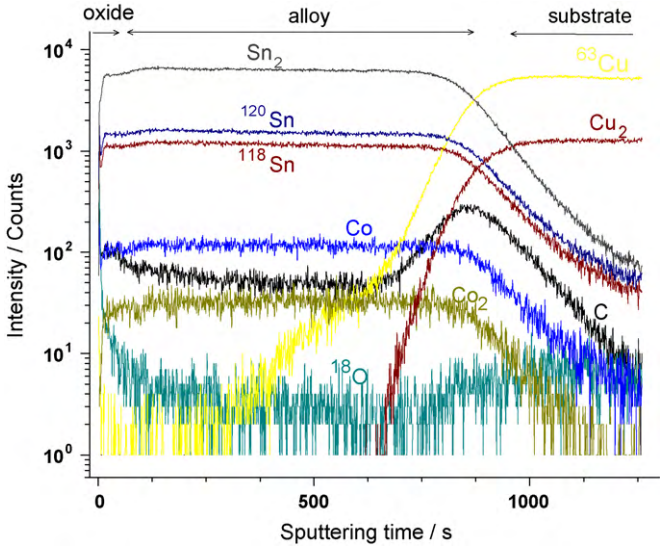

Fig. 4. ToF-SIMS negative ion depth profiles of a pristine Sn–Co alloy sample.

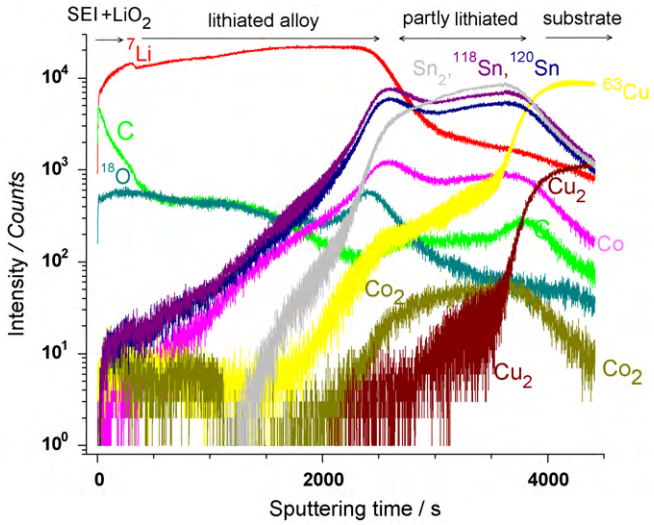

Fig. 5. ToF-SIMS negative ion depth profiles of a Sn–Co alloy anode discharged in 1 M $LiClO_4$/PC.

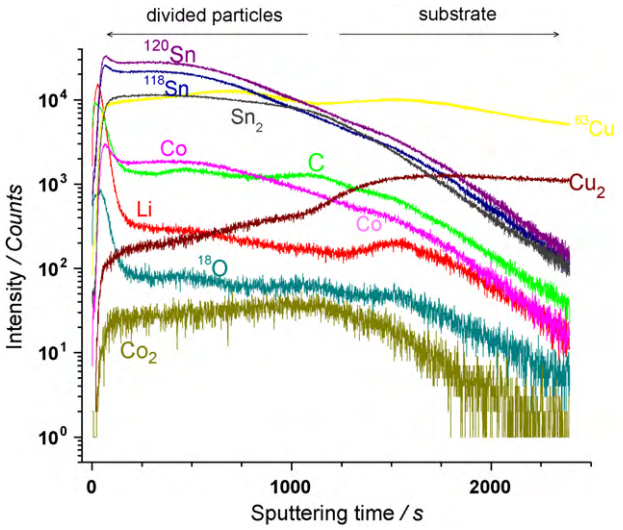

Fig. 6. ToF-SIMS negative ion depth profiles of a Sn–Co alloy anode discharged–charged in 1 M $LiClO_4$/PC.

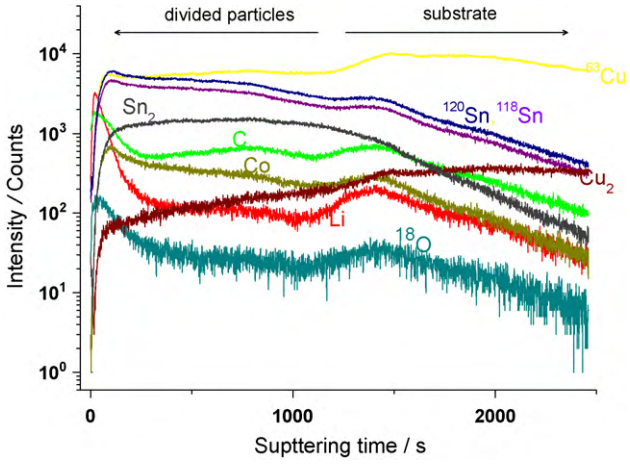

Fig. 7. ToF-SIMS negative ion depth profiles of a Sn–Co alloy anode discharged/charged ten times in 1 M $LiClO_4$/PC.

Several regions can be identified on the pristine Sn–Co sample (Fig. 4). The very first seconds of sputtering are characterized by a gradual increase of the signal of the higher intensity ions. This corresponds to the time needed to reach stationary conditions. In the first ~100 s of etching, the $^{18}O^-$ intensity decrease marks the surface oxide region identified by XPS. After ~100 s, the intensity plateaus of the Sn- and Co-containing ions mark the Sn–Co alloy region. The constant intensities of all Sn and Co signals imply a homogenous in-depth composition of the electroplated Sn–Co alloy layer. At ~750 s, the intensity of the Sn- and Co-containing ions starts to decrease while that of the Cu_2^- ions starts to increase. This marks the beginning of the alloy/substrate interfacial region. Such variation is observed until ~1000 s at which the Cu signal is stable, thus marking the end of this interfacial region. One can notice a hump in the C^- ion curve at ~850 s coinciding with the middle of the alloy/substrate interfacial region. It demonstrates the C contamination of the Cu surface before electroplating. It can be noticed that the intensity of the $^{63}Cu^-$ ions starts to increase before reaching the alloy/substrate region, suggesting the presence of pinhole defects and/or cavities in the alloy layer.

Fig. 5 displays the negative ion depth profile of a lithiated Sn–Co alloy sample prepared by galvanostatic discharge at 0.02 V. The sputter time to reach the interface with the Cu substrate, still marked by a C^- hump, has increased markedly to 3700 s, evidencing the volume expansion of lithiated Sn–Co alloy.

At least three regions can be distinguished prior to the alloy/substrate interfacial region. The first region, extending up to ~200 s is characterized by the intensity decrease of the C^- ions. This region is assigned to the SEI layer. The intensity increase of the Li-containing ions and the stable intensity of $^{18}O^-$ ions suggest a sub-layer in this region corresponding to the surface oxide possibly converted to Li_2O. The very low intensities of Sn- and Co-containing ions confirm the XPS results obtained on the lithiated sample.

In the next region extending up to ~2500 s, the intensities of Sn- and Co-containing ions increase while that of the Li-containing ions is nearly stable, which marks the lithiated part of the alloy layer ($Li_xSn + Co$, $x < 4.4$). In this region, the C^- ion intensity is higher than on the pristine sample, indicating an increase content of the decomposition products of the electrolyte, which suggests that the SEI layer fill the cracks in the Li_xSn alloy that are most likely generated by volume expansion. Cracking of the alloy layer is also indicated by the $^{63}Cu^-$ ion profile which, although of very low intensity, is more intense than on the pristine sample in the outermost region. After a maximum at 2600 s, the intensities of Sn- and Co-containing ions remain stable before reaching the substrate interface while those of the Li-containing ions decrease, marking an alloy region only partially lithiated. The formation of two sub-layers, i.e. a Li-rich outer sub-layer and an essentially non-lithiated inner sub-layer, starting from the initially homogeneous alloy layer reflects an incomplete alloying reaction limited by an intermediate barrier layer between the two sub-layers. The increase of the Co_2^- ion intensity from ~1800 s, i.e. before reaching the intermediate barrier layer, suggests that this dense intermediate barrier may consist predominantly of Co that could inhibit the diffusion of lithium to the inner sub-layer. Such a barrier layer, also observed on a lithiated Cr_2O_3 anode [38], is mainly built up by the component that acts as an inactive host of lithium, and thus hampers further alloying. This phenomenon restricts the discharge capacity to a value lower than the theoretical one [11,22,23,26]. In our experiment, the initial discharge capacity was 73% of theoretical value.

Fig. 6 shows the negative ion depth profiles of the Sn–Co anode after the first discharge/charge cycle. A significant difference consists in a gradual instead of a steep change of the ion intensities, which makes difficult the delimitation of the alloy/substrate interface. A break in the Cu_2^- and $^{63}Cu^-$ ion profile is observed at ~1100 s, which suggests that the sputtering has reached the interface between the Sn–Co alloy layer and the Cu substrate, and that the sputtering time on the Sn–Co alloy layer has been decreased to ~1100 s. This result implies a volume shrink of the Sn–Co alloy in comparison with the lithiated state. However, it presents still a volume expansion compared to the pristine state demonstrating the irreversibility of the morphological changes of the electrode. The second remarkable difference is the increased intensity of the Cu-containing ions right after the SEI layer region (i.e. after ~200 s). This corresponds to further cracking and voiding of the delithiated alloy layer exposing the Cu substrate. After the first volume expansion/shrink, the electroplated material develops then a cracked structure of Sn–Co alloy particles covered by the SEI layer. The Li-containing ion profiles parallel the C^- ion profile, demonstrating that most lithium ions are extracted from the alloy and that the dealloying reaction is quasi-reversible.

The negative ion depth profiles of the Sn–Co sample after 10 galvanostatic discharge/charge cycles are shown in Fig. 7. The breaks in the Cu-containing ion profiles appear at ~1100 s, which indicates that the sputtering time of the Sn–Co alloy layer remains ~1100 s. This result implies that no noticeable difference exists between the samples subjected to 10 charge–discharge cycles and only one cycle. It is obvious from these data that the Sn–Co alloy layer does not exfoliate after the changes produced by the first cycle, which is consistent with the stable capacity measured by electrochemistry. However, the Cu^- profile exhibits a higher intensity than the Sn^- profile, demonstrating a severe splitting up of the Sn–Co film into particles when the electrode has been subjected to multi-cycling. It can be also seen that the initial decreases of the C- and Li-containing ions are less sharp (i.e. slower) after 10 cycles than those measured with the sample subjected to only 1 cycle. This is consistent with an increased average content of the electrolyte reductive product due to the splitting up process. Still, it should be mentioned that the SEI layer covering each Sn–Co particle possibly becomes thinner on the multi-cycled sample, as suggested by the XPS results where the tin signal can be then detected.

The morphology variations of cycled tin-based alloy anodes have been previously investigated by SEM, which showed the formation of cracks and the delamination of active material layers during cycling [1,11,13]. The cracks allow the electrolyte to penetrate between the copper current collector and the alloy layer, where it is reduced to electronically insulating products. For Sn–Co films on rough Cu foil [11,13], it was reported that the film cracks and divides into an island-like structure after the 1st discharge–charge cycle, and that the islands become smaller and the film roughness increases with cycle number.

4. Conclusion

Sn–Co alloy films prepared by electroplating on a copper substrate were used as anode of lithium ion battery. The interfacial processes and bulk reactions of the Sn–Co anode were investigated by combining electrochemical lithiation and delithiation in 1 M $LiClO_4$/PC and analysis by XPS and ToF-SIMS in ultra-high-vacuum. The results illustrated that the pristine Sn–Co alloy specimens were covered by a Sn-rich oxide layer. A solid electrolyte interphase (SEI) layer is built up at the surface of cycled samples as evidenced by XPS. It was shown that the SEI layer is constituted of a mixture of Li_2CO_3, $ROCO_2Li$, lithium oxalates, and/or ROLi, and its chemical composition is varied with increasing Li_2CO_3 content during the electrochemical charge-discharge cycling process. Multi-cycling also fractures the SEI layer as indicated by the re-appearance of the Sn3d core level after 20 cycles. Trapping of negatively charged Sn (likely alloyed to Li) at the surface of the Sn–Co alloy layer is then observed in the delithiated state.

ToF-SIMS depth profiling revealed an incomplete initial alloying process of lithium with tin, which divides the electroplated layer into a highly lithiated outer part (Li_xSn) and an essentially non-lithiated inner part. The formation of a Co layer in the discharge process limits further mass transport of lithium. Volume expansion/shrink resulting from the alloying/dealloying reactions with lithium was also evidenced by TOF-SIMS. Such process cracks the initially homogeneous structure of the Sn–Co layer, and most likely splits up the Sn–Co film into alloy particles. The SEI layer also builds up at the new surface created in the cracked film.

Acknowledgments

This work was partially supported by the Special Funds for Major State Basic Research Project of China (Grant No. 2009CB220102) and NSFC (Grant Nos. 20833005 and 20773102). Region Ile-de-France is acknowledged for partial support for the XPS and ToF-SIMS equipments.

References

[1] M. Winter, J.O. Besenhard, Electrochim. Acta 45 (1999) 31–50.
[2] R.A. Huggins, J. Power Sources 81–82 (1999) 13–19.
[3] O. Mao, R.L. Turner, I.A. Courtney, B.D. Fredericksen, M.I. Buckett, L.J. Krause, J.R. Dahn, Electrochem, Solid State Lett. 2 (1999) 3–5.
[4] J.O. Besenhard, J. Yang, M. Winter, J. Power Sources 68 (1997) 87–90.
[5] N. Tamura, R. Ohshita, M. Fujimoto, M. Kamino, S. Fujitani, J. Electrochem. Soc. 150 (2003) A679–A683.
[6] Z. Wang, W.H. Tian, X.H. Liu, R. Yang, X.G. Li, J. Solid State Electrochem. 180 (2007) 3360–3365.
[7] F. Wang, M.S. Zhao, X.P. Song, J. Power Sources 175 (2008) 558–563.
[8] W.J. Cui, F. Li, H.J. Liu, C.X. Wang, Y.Y. Xia, J. Mater. Chem. 19 (2009) 7202–7207.
[9] G.F. Ortiz, R. Alcantara, I. Rodriguez, J.L. Tirado, J. Electroanal. Chem. 605 (2007) 98–108.
[10] J. Hassoun, G. Mulas, S. Panero, B. Scrosati, Electrochem. Commun. 9 (2007) 2075–2081.
[11] N. Tamura, Y. Kato, A. Mikami, M. Kamino, S. Matsuta, S. Fujitani, J. Electrochem. Soc. 153 (2006) A1626–A1632.
[12] H. Guo, H.L. Zhao, X.D. Jia, X. Li, W.L. Qiu, Electrochim. Acta 52 (2007) 4853–4857.
[13] N. Tamura, Y. Kato, A. Mikami, M. Kamino, S. Matsuta, S. Fujitani, J. Electrochem. Soc. 153 (2006) A2227–A2231.
[14] H. Kim, J. Cho, Electrochim. Acta 52 (2007) 4197–4201.
[15] M. Valvo, U. Lafont, L. Simonin, E.M. Kelder, J. Power Sources 174 (2007) 428–434.
[16] H. Kim, J.P. Cho, J. Electrochem. Soc. 154 (2007) A462–A466.
[17] T. Tabuchia, N. Hochgatterer, Z. Ogumi, M. Winter, J. Power Sources 188 (2009) 552–557.
[18] A.D.W. Todd, R.E. Mar, J.R. Dahn, J. Electrochem. Soc. 153 (2006) A1998–A2005.
[19] P.P. Fergusona, M.L. Martinea, R.A. Dunlap, J.R. Dahn, Electrochim. Acta 54 (2009) 4534–4539.
[20] P.P. Ferguson, M. Rajora, R.A. Dunlap, J.R. Dahn, J. Electrochem. Soc. 156 (2009) A204–A208.
[21] S.I. Lee, S. Yoon, C.M. Park, J.M. Lee, H. Kim, D. Im, S.G. Doo, H.J. Sohn, Electrochim. Acta 54 (2008) 364–369.
[22] J.J. Zhang, Y.Y. Xia, J. Electrochem. Soc. 153 (2006) A1466–A1471.
[23] X.Y. Fan, F.S. Ke, G.Z. Wei, L. Huang, S.G. Sun, J. Alloys Compd. 476 (2009) 70–73.
[24] P.A. Connor, J.T.S. Irvine, Electrochim. Acta 47 (2002) 2885–2892.
[25] A.D.W. Todd, R.A. Dunlap, J.R. Dahn, J. Alloys Compd. 443 (2007) 114–120.
[26] C.M. Ionica-Bousquet, P.E. Lippens, L. Aldon, J. Olivier-Fourcade, J.C. Jumas, Chem. Mater. 18 (2006) 6442–6447.
[27] R.A. Dunlap, O. Mao, J.R. Dahn, Phys. Rev. B 59 (1999) 3494–3500.
[28] K.K.D. Ehinon, S. Naille, R. Dedryvere, P.E. Lippens, J.C. Jumas, D. Gonbeau, Chem. Mater. 20 (2008) 5388–5398.
[29] R. Dedryvere, S. Leroy, H. Martinez, F. Blanchard, D. Lemordant, D. Gonbeau, J. Phys. Chem. B 110 (2006) 12986–12992.
[30] S. Naille, R. Dedryvere, H. Martinez, S. Leroy, P.E. Lippens, J.C. Jumas, D. Gonbeau, J. Power Sources 174 (2007) 1086–1090.
[31] S. Leroy, H. Martinez, R. Dedryvere, D. Lemordant, D. Gonbeau, Appl. Surf. Sci. 253 (2007) 4895–4905.
[32] X.M. Wang, T. Hironaka, E. Hayashi, C. Yamada, H. Naito, G. Segami, Y. Sakiyama, Y. Takahashi, K. Kibe, J. Power Sources 168 (2007) 484–492.
[33] S.W. Song, S.W. Baek, Electrochim. Acta 54 (2009) 1312–1318.
[34] J.T. Li, S.R. Chen, X.Y. Fan, L. Huang, S.G. Sun, Langmuir 23 (2007) 13174–13180.
[35] S. Leroy, F. Blanchard, R. Dedryvere, H. Martinez, B. Carre, D. Lemordant, D. Gonbeau, Surf. Interface Anal. 37 (2005) 773–781.
[36] S. Oswald, K. Nikolowski, H. Ehrenberg, Anal. Bioanal. Chem. 393 (2009) 1871–1877.
[37] J. Swiatowska-Mrowiecka, S. de Diesbach, V. Maurice, S. Zanna, L. Klein, E. Briand, I. Vickridge, P. Marcus, J. Phys. Chem. C 112 (2008) 11050–11058.
[38] J.T. Li, V. Maurice, J. Swiatowska-Mrowiecka, A. Seyeux, S. Zanna, L. Klein, S.G. Sun, P. Marcus, Electrochim. Acta 54 (2009) 3700–3707.
[39] R. Alcantara, G.F. Ortiz, P. Lavela, J.L. Tirado, W. Jaegermann, A. Thissen, J. Electroanal. Chem. 584 (2005) 147–156.
[40] J. Swiatowska-Mrowiecka, V. Maurice, S. Zanna, L. Klein, P. Marcus, Electrochim. Acta 52 (2007) 5644–5653.
[41] I. Porqueras, G. Viera, J. Marti, E. Bertran, Thin Solid Films 343–344 (1999) 179–192.
[42] J. Swiatowska-Mrowiecka, F. Martin, V. Maurice, S. Zanna, L. Klein, J. Castle, P. Marcus, Electrochim. Acta 53 (2008) 4257–4266.
[43] H. Ota, T. Akai, H. Namita, S. Yamaguchi, M. Nomura, J. Power Sources 119–121 (2003) 567–571.
[44] V. Yufit, D. Golodnitsky, L. Burstein, M. Nathan, E. Peled, J. Solid State Electrochem. 12 (2008) 273–285.
[45] D. Alamarguy, J.E. Castle, M. Liberatore, F. Decker, Surf. Interface Anal. 38 (2006) 847–850.
[46] A. Lebugle, U. Axelsson, R. Nyholm, N. Martensson, Phys. Scr. 23 (1981) 825–827.
[47] K. Xu, G.R.V. Zhuang, J.L. Allen, U. Lee, S.S. Zhang, P.N. Ross, T.R. Jow, J. Phys. Chem. B 110 (2006) 7708–7719.
[48] G.V. Zhuang, K. Xu, T.R. Jow, P.N. Ross, Electrochem. Solid-State Lett. 7 (2004) A224–A227.
[49] Q.H. Wu, J. Song, J.C. Lia, Surf. Interface Anal. 40 (2008) 1488–1492.
[50] W.J. Kim, W.H. Koo, S.J. Jo, C.S. Kim, H.K. Baik, J. Lee, S. Im, Appl. Surf. Sci. 252 (2005) 1332–1338.